⋆ *Based on observations collected at the SEST 15m telescope (Chile).*

⋆ (†)

Mon. Not. R. Astron. Soc. **000**, 000–000 (0000) Printed 1 February 2008

1.25 mm Observations of a Complete Sample of IRAS Galaxies: (II) Dust Properties (†)

Paola Andreani[1] and Alberto Franceschini[2]

[1] *Dipartimento di Astronomia di Padova, vicolo dell'Osservatorio 5, I-35142 Padova, Italy. e-mail: andreani@pdmida.pd.astro.it and European Southern Observatory, D-85748 Garching, Germany*

[2] *Dipartimento di Astronomia di Padova, vicolo dell'Osservatorio 5, I-35142 Padova, Italy. e-mail: franceschini@astrpd.pd.astro.it*

Accepted ..... Received ..... in original form January 15th 1996

ABSTRACT

We present 1.25 mm continuum data for a southern galaxy sample selected from the IRAS PSC and complete to $S_{60} = 2\ Jy$. Two thirds of the galaxies have been detected and significant limits on the remaining objects have been set. We find, on a statistical basis, indications that the dust emission in these galaxies is somewhat more centrally concentrated than that of the optical light, possibly tracing a higher metal content in the inner galactic regions. This result also allows to estimate the aperture corrections to the millimetric data. The latter, together with IRAS photometric data, have been used to compare the broad-band FIR/mm spectra with a simple dust model. According to their far-IR/mm spectrum, the sample galaxies show a dichothomy: almost half of the objects, those displaying bright 25-60 μm fluxes ascribed to warm dust residing in *starburst* regions, are characterized by higher values of the bolometric (optical + FIR) luminosity, of the dust-to-gas mass ratio, of the dust optical depths and of the overall extinction. A complementary class of objects dominated by cold dust (*cirrus*) shows opposite trends. Because of the favourable observational setup, selection wavelength and completeness, we believe these data provide an exhaustive and unbiased view of dust properties in spiral galaxies.

Key words: galaxies: ISM - galaxies: photometry - galaxies: spirals, starburst - ISM: dust, extinction - infrared: ISM: continuum

1 INTRODUCTION

Observations of diffuse dust in galaxies provide important information on some basic questions about their present structure and past history. Even minor amounts of absorbing dust play a crucial role in shaping the galaxy's broad-band e.m. emission. Any inferences about structural properties, such as the global baryonic content, its spatial distribution, and the presence of a dynamically dominant non-baryonic component, rely on our ability to account for the missing fraction of light in optical searches (Disney, Davies and Phillips, 1989; Choloniewski 1991; Burstein, Haynes & Faber 1991; Huizinga & van Albada 1992; Giovannelli et al. 1994; Valentijn 1994; Peletier et al. 1995). Are we missing significant amounts of luminous matter because of the effects of dust extinction? How much severe are the corresponding selection effects?

Dust is also an important tracer of the activity of stellar populations in galaxies. By cumulating the products of all stellar generations, diffuse dust provides an integrated view of the past history of the object.

There is a tendency, as of today, to consider the innermost parts of late-type galaxy discs close to optical thickness, but for the outer regions the question cannot yet be settled with present data. Fundamental questions of extragalactic astronomy, e.g. the calibration of distance indicators, are affected by this lack of knowledge.

Traditional approaches to investigate dust in galaxies rely on either *(a)* indirect estimates based on dust extinction effects in the optical and near-IR (e.g. White & Keel 1992; James & Puxley 1993; Block et al. 1994), or *(b)* direct measurements of dust emission from FIR/mm observations. Neither have provided conclusive results at the moment. The former method is based on rather model-dependent and controversial assumptions about the broad-band optical-IR spectrum of various galactic components. The latter method, on the other hand, still lacks a large enough statistical basis and suffers from the observational uncertainties of the mm data.

IRAS survey data, although having provided the starting point for studies of galaxy emission at long wavelengths, are not enough by themselves to fully characterize the dust content and emission properties, because of its limited sen-

sitivity, spatial resolution, and spectral coverage. In particular, dust colder than 20 K at large radial distances, whose existence is currently matter of so much controversial discussions (Rowan-Robinson, 1992; Valentijn, 1994; Block et al., 1994), can only be sampled at $\lambda > 100\mu m$ (Chini et al., 1986; Thronson et al., 1987; Stark et al., 1989; Andreani and Franceschini, 1992), where direct observations are still limited to a handful of objects.

This paper reports on a millimetric continuum survey of a complete sample of IRAS galaxies performed at 1.25 *mm* with the 15m Submillimeter ESO-Swedish telescope (SEST). A preliminary report on these observations has been given by Franceschini and Andreani (1995).

The SEST telescope was chosen as it provided the best compromise between detector sensitivity and spatial resolution. The $24''$ FWHM of the SEST beam at 1.25 *mm* and the average optical extent of the sample galaxies match favourably, so that the beam-aperture corrections needed to compare with the IRAS survey data are not as severe as for other observational setups.

Observations at such long wavelengths, made possible by the high sensitivity of the used bolometer system, ensure that all possible dust components with temperatures down to the fundamental limit of $T \simeq 3\ K$ set by the cosmic background radiation are properly sampled. The reference to a complete flux-limited sample ensures a minimal exposure to the effects of bias, hence allowing any kinds of statistical tests to be applied (determinations of IR-mm bivariate luminosity distributions, luminosity functions and volume emissivities: Franceschini and Andreani, 1996, work in progress). Finally, the adoption of a far-IR selected sample, rather than of an optical one, makes us confident that the whole phenomenology of dust effects in galaxies is properly sampled.

Section 2 is devoted to the present observations and discusses the issue of the extent of the millimetric emission and the beam-aperture corrections. Section 3 reports results from the best-fit to the observed spectra with a dust model and the inferred dust properties for our sample, while the discussion is deferred to §4.

2 OBSERVATIONS AND DATA ANALYSIS

2.1 The sample

The galaxy sample under investigation was selected from the IRAS Point Source Catalogue and is complete to the flux limit of $S_{60\mu m} = 2$ Jy. It consists of 30 galaxies with morphological types from S0/a through Scd, within the sky region $21^h < \alpha(1950) < 5^h$ and $-22.5^\circ < \delta < -26.5^\circ$. For most of these galaxies PSC data also at 100, 25 and 12 μm were available. Distances (mostly from distance indicators, otherwise derived using redshift data for $H_0 = 75$) cover the range from $d \simeq 20$ to $\simeq 200$ Mpc. Half-optical-light diameters A_e are typically within $A_e \simeq 10''$ to $\simeq 40''$, four exceptionally close galaxies having $A_e \sim 100''$. The volume test ($< V/V_{max} >= 0.45 \pm 0.06$) ensures the sample completeness.

Table 1 reports some relevant information (name, coordinates, distances, optical dimensions, blue magnitudes and morphological types) for the sample galaxies. The data have been taken from the Lyon-Meudon Extragalactic Database (LEDA), the NASA Extragalactic Database (NED) and the IRAS PSC (Moshir et al., 1989). Optical photometric data have been taken from the ESO-LV catalogue (Lauberts & Valentijn, 1989).

Table 1

2.2 The bolometer observations

The sample has been observed at 230 GHz during various campaigns from 1990 to 1993 with the SEST 15m telescope feeding a ^{3}He-cooled bolometer of the MPIfR (Kreysa 1990). The diffraction-limited beam size is $24''$ (FWHM). Beam-switching is achieved by chopping ON-OFF the source and nodding the telescope, which results in a three-beam modulation on and off the source. The beam separation was set at $70''$. The pointing accuracy was most of the time $2''$ and was checked each half a hour, by pointing a nearby radio-loud quasar. Each source was observed $n \times 200$ seconds, with n depending on the expected 1.25 *mm* intensity (approximately evaluated by extrapolating the IRAS $100\mu m$ flux using a modified thermal spectrum with spectral indices of dust opacity between 1 and 2).

The atmospheric transmission was monitored by frequent skydips. Uranus, Mars and Neptune were used as primary calibrators and the pointing quasars as secondary ones. The overall accuracy of the measured fluxes (which we estimate to be between 10 and 30%) strongly depends on the atmospheric conditions. A more detailed description of the observing procedure can be found in Andreani & Franceschini (1992) and Andreani (1994).

Table 2 reports our observed 1.25 *mm* fluxes (cols. 4 and 5), together with the IRAS at 25, 60 and 100 μm fluxes (cols. 1, 2, 3), all corrected for color and K-correction following Smith et al. (1987). In the lack of a detection a 3 σ upper limit to the flux is reported.

Table 2

2.3 Beam-aperture corrections: the size of galaxies at $\lambda = 1.25\ mm$

Corrections to the observed millimetric fluxes, to account for the beam aperture of the telescope being comparable to or even smaller than the angular size of the sources, are crucial to estimate the global mm emission and to compare it with the total fluxes provided by the IRAS survey. Such a difficult evaluation is one of the main reasons preventing so far to reach reliable conclusions about dust emission in galaxies.

Up to now our knowledge on the dust distribution in galaxies mostly relied on IRAS data, whose basic results are briefly summarized in the following.

Light profiles similar, on average, in the far-IR and optical band were inferred from a direct comparison of blue-band, $\lambda = 50$ and 100 μm data using the IRAS CPC

(Chopped Photometric Channel) instrument by Wainscoat *et al.* (1987) on three nearby edge-on spirals and by van Driel et al. (1995) on 55 nearby spirals. A study of a sample of extended galaxies, partially resolved by IRAS (Rice *et al.* 1988), shows that the mean ratio of the far-IR (60 μm) D_{IR} to blue-light D_B isophotal diameters turns out to be 0.98±0.25. This implies that on average galaxies have far-IR extensions comparable to the blue ones. A similar result is found by Xu & Helou (1995) for M31. They combined FIR and UV data of M31 and a dust heating/cooling model, to study the extinction in the disc of this galaxy. The overall distribution of V-band optical depth in this galaxy is rather flat and it is very tight correlated with the HI column density. There are IRAS objects, however, where the IR emission seems to be more centrally concentrated than that of the blue light.

First attempts to map mm dust emission have been recently done by Chini & Krügel (1993) and Chini et al. (1995), who have shown that the distribution of the millimetric light is similar to the optical one and argue that for the observed objects cold dust emission is extended as far as the blue light.

Two main advantages distinguish our sample: the majority of the objects are relatively distant and have small angular sizes in the optical. Furthermore, the SEST antenna has a a relative large beam-width with respect to other millimetric telescopes (JCMT and IRAM). In spite of this, aperture corrections may still turn out to be significant and deserve particular attention. The solution we devised is the following. For some of the optically most extended sources (0300–23, 0335–24, 2217–24, 2233–26) we have performed a rough mapping by integrating on four points, one beam-width distant, around the galaxy center. The fluxes listed in Table 2 have been obtained by adding the contributions of each observed position. This allows at least to reduce the large aperture corrections for these sources.

The galaxy 0045-25 (NGC 253) was not observed by us and the flux listed in Table 2 is taken from Chini et al. (1984). These authors performed aperture photometry with a beam of width of 3.9′ and measured a flux of 4.4±1.7 Jy. The inner region (2′x3′) of this object was also mapped at 1.25 *mm* by Krügel et al. (1990). These authors estimate a total flux in this inner region of 1.7±0.2 Jy. However, this well-known object is very nearby and therefore quite extended in the optical (27.4′x6.8′), it is very likely that both measurements have underestimated the real emission.

More generally, our adopted procedure was to test three different hypotheses about the geometrical distribution of the millimetric flux. (1) Sources are point-like objects, hence no beam-aperture correction is to be applied; (2) the radial distribution of the millimetric light is exponential with a scale-length $\alpha_{\rm mm}$ equal to one third of the optical one: $\alpha_{\rm mm} = \alpha_0/3$ (case of dust emission more concentrated than the star-light) and (3) the dust emission follows that of the optical light ($\alpha_{\rm mm} = \alpha_0$).

The model surface brightness distributions corresponding to the three cases have been convolved with the telescope beam shape following Andreani and Franceschini (1992). Results of these aperture corrections to the observed mm fluxes are reported in Table 2. In columns 6 and 7 the fluxes corrected according to hypothesis (2) are listed, and in columns 8 and 9 those corrected according to hypothesis (3). Note that for case (2) the aperture-correction turns out to be 20% on average of the observed mm flux (the largest correction is a factor 3 for 0311-25). An average correction of roughly a factor 2 is instead required according to hypothesis (3).

We have tested further the three different hypotheses on the *mm* light distribution against our data as follows. Figures 1a and 1b are plots of the ratios of the 1.25 *mm* to the 60 and 100 μm fluxes versus galaxy distance and diameter, with $S_{1.25}$ corrected according to the three above mentioned hypotheses. The two lines in each panel of Fig. 1 correspond to the ± 1 σ regression fits obtained with a "survival analysis" technique.

We see in Fig. 1a that hypothesis (3) in particular implies a dependence of the average flux ratio with distance which is significant at the 3.5σ level for the 100 μm (and 5.5σ for the 60 μm match). This is of course not expected, since all flux measurements have already been K-corrected. We are led to conclude that the hypothesis of the presence of *emitting* dust at large radial distances appear to be inconsistent with our data, as detailed in Sect. 3 below. Instead, the case for a higher concentration of dust emission, with $\alpha_{\rm mm}$ between $\alpha_o/3$ and $\alpha_o/2$, is fully supported. An even stronger indication in favour of the latter assumption is observed in Fig. 1b, where the mm-IR flux ratios versus the galaxy effective diameter is shown.

Figure 1. (a) Millimetric to far-IR flux ratios versus galaxy distance. Top panels compare with the 100 μm flux, bottom panels with the 60 μm. In panels to the left the mm data have been corrected for beam-aperture assuming point-sources, central panels assume a mm scale-length of 1/3 of the optical one, right-hand side panels assume the same distribution for the mm and optical light. Panel (b) same as (a), but for the far-IR flux ratios versus galaxy diameter.

The millimeter fluxes used hereafter were therefore corrected for the effect of beam-aperture according to the assumption $\alpha_{\rm mm} = \alpha_0/3$. Our mm data for all the sample galaxies, as well as the complementary IRAS fluxes, are plotted in Figure 2. Best-fits of a dust emission model discussed in the next Section also appear in the figure.

3 THE DUST CONTENT OF GALAXIES

3.1 The dust model

Data at millimeter wavelengths, improving on the spectral dynamic range with respect to the IRAS survey data, add significantly to our knowledge of dust properties in infrared galaxies. No dust component, at whichever temperature, is expected to escape a combined mm-IRAS survey.

FIR spectra of spiral galaxies are schematically interpreted as due to thermal re-radiation from dust present in three main galactic environments: *(a)* dust grains heated by the general interstellar radiation field ("cirrus" emission including cold dust and small transiently-heated hot dust grains), *(b)* dust heated by hot stars in extended HII regions, and *(c)* dust in compact HII regions and molecular clouds. The "cirrus" component has been modeled following the recipes by Rowan-Robinson (1986, 1992; hereafter RR86, RR92). The model predicts the existence of nine grain types: amorphous carbon and silicate grains of size $a = 0.1\ \mu m$, graphite and silicate of 0.01 and $0.03\mu m$ size, very small ($a = 0.002$ and $0.0005\ \mu m$) transiently-heated graphite grains, and finally a component of very large amorphous grains with radius $a = 30\ \mu m$ to account for the observed submillimeter properties. The mixture and grain properties have been optimized by RR92 to reproduce all basic observables (extinction law, absorption properties of the ISM towards various galactic regions) over the entire 1 mm to 0.1 μm spectral range.

For normal grains the emission temperature is assumed to attain equilibrium (the thermal capacity is large enough with respect to the energy of the field photons), and is estimated from an energy balance equation between the emitted and absorbed photons (including the scattered fraction). On the contrary, very small grains, because of their small sizes, are not in thermal equilibrium with the impinging radiation field and their emission fluctuates according to their changes in temperature. Their thermal behaviour is described by a probability distribution function P(T), which has the approximated analytic expression given by Draine & Anderson (1985):

$$P(T) = \begin{cases} 6.680 \cdot T^{-2.75} & \text{if } 2.7 \leq T \leq 80 \quad a = 20\mathring{A}; \\ 0.168 \cdot T^{-2.75} & \text{if } 2.7 \leq T \leq 500 \quad a = 5\mathring{A} \end{cases}$$

Their scattering and absorbing properties for $\lambda > 0.1\mu m$ are those of $0.01\mu m$ grains scaled by a factor of $a/0.01$ (see below). In fact for small grains ($a \leq 0.1\lambda$) the extinction efficiency, Q_{ext}/a is independent of a.

For the warm dust in star-forming regions we have followed a simplified but successful approach as illustrated by Xu and De Zotti (1989) and Conte (1993). The star-forming region is modeled as a volume uniformly filled with hot stars, dust and radiation, and is assumed to be optically thin at least for $\lambda > 20\ \mu m$. The same grain mixture as for the

Figure 2. FIR/mm spectra of the sample objects. In each panel the name, the total FIR/mm luminosity and dust mass (estimated from the dust model) are shown. Solid lines are the global fitted spectrum, including two dust components: (1) the *cirrus* (dashed line), and the *starburst* component (dot-dashed line).

"cirrus" component is adopted, but very small grains are assumed to be destroyed by the intense radiation field.

3.2 The dust emissivity

The total emissivity due to the hot, warm and cold components is given respectively by:

$$4\pi\epsilon_T(\nu) =$$

$$\sum_{i=1}^{2}\chi_c\int 4\pi N_{gr,H}(a_i)Q_{ext}(a_i,\nu)\pi a_i^2 P(T)B_\nu(T)dT+$$

$$\sum_{i=1}^{4}4\pi N_{gr,H}(a_i)Q_{ext}(a_i,\nu)\pi a_i^2 B_\nu(T_i)+ \qquad (1)$$

$$\sum_{i=1}^{7}4\pi N_{gr,H}(a_i)Q_{ext}(a_i,\nu)\pi a_i^2 B_\nu(T_i)$$

$N_{gr,H}$ are the number of grains per H atom, $Q_{ext}(a_i,\nu)$ are the extinction efficiencies, $B_\nu(T_i)$ is the black body spectrum at the equilibrium temperature and χ_c is the ratio between the intensity of the interstellar radiation field and that of the field in the solar neighbourhood. This latter has been taken by Mathis et al. (1983). The sum of the warm component runs over only four of the seven components, because for warm environments, such as those of HII regions, the differences in optical properties of grains with equal dimensions and different chemical compositions can be neglected. In this case, the averaged extinction efficiencies and total abundances have been put in eq.(1). The UV absorbing efficiency for these grains was taken equal to 1 and the radiation field was assumed uniform inside the HII regions.

The equilibrium temperatures for all grains of both the "cirrus" and starburst components are uniquely determined by solving the balance equations with the the average radiation field intensity, χ_c, in the cold "cirrus" and the intensity illuminating the warm dust in star-forming regions, χ_w, as free parameters. The third parameter used in the model is the light fraction f_w at 100 μm contributed by warm dust to the galaxy spectrum. These three parameters fully describe the dust model. The fitting procedure assumes that the 1.25 mm flux is dominated by cold dust belonging to the "cirrus" component, which mostly defines χ_c. The 60 and 25 μm data mostly define the other two parameters.

3.3 Dust distribution in galaxy discs

We test in this section which spatial distributions of dust in galaxy discs correspond to the surface brightness distribution of the millimetric emission inferred in §2 from our observations (though we recall that this distribution has been indirectly estimated using a statistical argument, and then may be prone to unaccounted systematic effects). We expect, in general, that because of the scaling with radius of the interstellar radiation field and hence of the dust emissivity, the mm light should be more centrally concentrated than the optical.

Figure 3. Integrated galactic light as a function of the galactic radial distance. The solid curve corresponds to the starlight, the dashed curve to the dust emission found by assuming the dust distribution follows that of the stars. The dotted curve represents the integrated dust emission with a dust distribution more concentrated that that of stars (the scale-length in this case is one third of the optical).

We have modelled the galactic interstellar radiation field as an exponential scaling with the radial distance in the disc $I = I_0 \cdot exp(-r/r_d)$ (with r_d=3.5 kpc, e.g. Reid 1994), i.e. closely following the distribution of stars. We have then computed the dust emission according to our adopted dust model, assuming *(a)* that the dust distribution is more centrally concentrated (with scale-length of one third of that of stars) and *(b)* alternatively that it follows the starlight distribution.
The integrated surface brightness distributions resulting from this calculation are shown in Figure 3, the solid curve referring to the interstellar radiation field, the dashed one to a mm emission resulting from a dust distribution equal to that of stars, the dotted curve corresponding to the case of a dust scale-length of one third of that of stars. The corresponding ratios of the optical scale-length, α_o, to the mm-light scale-length, α_{mm}, are 1.3 in the first case and 3.1 for the second. Obviously, for a centrally concentrated dust distribution, the key factor is α_{mm} rather than α_o. This implies that the spatial distribution of the mm light that we have inferred roughly coincides with the real underlying dust distribution.

3.4 Best-fit dust models to the observed spectra

The best-fit spectra for the sample galaxies are shown in Fig. 2. The adopted dust model, for a suitable choice of the parameters, reasonably reproduces the observed far-IR/mm broad-band spectra for all objects, a result which confirms and extends previous findings by RR92. The dashed line in Fig. 2 corresponds to the "cirrus" component, the dot-dashed ones to the starburst component.

For 16 galaxies in our sample the contribution of warm dust at 100 μm appears to be negligible, and sometimes not even required to improved the fit with a pure "cirrus" com-

ponent. We call these *"cirrus"-dominated* galaxies. On the other hand, 14 objects require high values of the warm dust fraction ($f_w \geq 0.3 \div 0.4$), and their spectrum at $\lambda < 100\ \mu m$ is dominated by the starburst component (the *starburst-dominated* galaxies). We then suggest that far-IR to mm data and a reliable dust model provide a straightforward way to classify galaxies according to their star formation activity. This allows a complementary classification tool with respect to the usual approach based on optical-UV spectrophotometry.

In each panel of Fig. 2 best-fit values for the total dust mass and the FIR luminosities are also reported. The latter have been computed by integrating the total FIR/mm spectrum. Dust masses for both cold and warm dust have been estimated following RR86's recipes for the mean density of grain material, while, for a given spectral fit, the total number of grains is set by the far-IR flux normalization. The mass of diffuse dust in the interstellar medium is found to be mostly contributed by the cold "cirrus" component (97.5% on average), with only a minor fraction of the mass resident in the starburst component. The dust fraction involved in the latter ranges from typically several percent for starburst galaxies to one percent in the inactive population. Figure 4 shows the average FIR/mm spectrum for 30 galaxies in our sample fitted with a two-dust component and the corresponding best-fit parameters of the dust model are listed in Table 3 (the reduced χ^2_ν is 0.68). Note that the starburst component contributes only a couple of percent on average of the total dust mass.

Table 3

The quoted dust masses should be taken as lower limits: some dust may be hidden at low enough temperatures, given the strong dependence of dust emissivity on temperature. We argue here that only very sensitive *mm* observations (like those presented here) can tackle it successfully. In fact, though the results from these fits are by no means unique, there is no room for large amounts of dust mass in the framework of the adopted model. The data are compatible with models having an additional very cold dust component illuminated by a very dim radiation field ($\chi_c = 0.5\chi_\odot$) and with a temperature distribution ranging from T$\sim$4 to 18 K. In this case this very cold component would bear 76.3 % of the total mass and the total average dust mass would be increased by 30%.
The largest amount of dust still allowed by our observed dust spectra may be computed assuming that all dust components are set to the fundamental temperature of 3 K (the corresponding radiation field would be $\chi_c = 0.01\chi_\odot$). The resulting mass of this very cold dust would include 90% of the total, which would be twice larger than our best-fit value. Then we estimate that our dust masses are correct within a factor of two, for the adopted dust model.

Figure 4. The average far-IR millimeter broad-band spectrum for the *median* galaxy in our sample. A two component model, including the *cirrus* (dashed line) and *starburst* (dot-dashed line) contributions with best-fit parameters $\chi_c = 11\chi_\odot$, $\chi_w = 120\chi_\odot$ (normalized to solar neighborhood) The flux normalization at 100 μm of the starburst component is $f_w = 0.3$. The physical parameters of dust grains are detailed in Table 3. The median value of the 100 μm flux for our sample galaxies is $S_{100} = 7.5\ Jy$.

3.5 Effects of dust extinction on the overall spectrum

An overall view of dust effects in our IR galaxy sample is summarized in Figure 5 in terms of extinction versus dust optical-depth. The observed B-band optical depth τ_B has been estimated from the total dust mass divided by the projected area within which we estimate to be resident the cold dust, i.e. the inner third of the optical radius (R_{25}), properly scaled with the axial ratio squared $(b/a)^2$ to account for the disk inclination. τ_B, which measures the amount of dust *available* to absorb the optical light, is compared in Fig. 5 with the quantity A_B measuring the overall *actual* effect of extinction. The average B extinction, A_B, has been estimated from the logarithmic ratio of the bolometric optical-UV luminosity from 0.1 to 10 μm (L_O) to the bolometric far-IR light (L_{FIR}, 10 to 1000 μm) (two objects are missing in Figure 5 because optical photometry is not available).

We see that the two galaxy classes, that we have defined are significantly segregated over this plane, the inactive "cirrus"-dominated objects being confined to lower values of dust optical depth ($\tau_B < 2$) and low extinction ($A_B \leq 1$). The active star-forming galaxies, on the contrary, are spread over much larger values in both axes. The predicted dependences for a screen, a slab, and a sandwich (with

Figure 5. Observed optical depth of dust τ_B versus the overall extinction A_B. τ_B is averaged within one third of the R_{25} radius. A_B is estimated by comparing the bolometric outputs in the optical and far-IR. Open and filled squares refer the the inactive *cirrus*-dominated and to the starbursting objects. The position marked by the symbol ($\odot$) corresponds to our Galaxy.

Figure 6. Best-fit of the dust model to spectral intensity data on our Galaxy (Puget 1989; Page et al. 1990; Wright et al. 1991). The data are fitted by a pure *cirrus* emission (no starburst emission), with $\chi_c = 8\chi_\odot$. The total dust mass is $M_d = 10^7\ M_\odot$. The dashed line corresponds to the best-fit by Wright et al. (1991).

zero scale-height of dust) model are shown for comparison (see Disney et al., 1989). Appreciable amounts of dust and extinction seem to characterize only a population of starbursting galaxies, with typical values of the effective optical depth τ_B of 1 to 20 in the inner one third of the optical radius. However, only for a minority of these starbursts (4/13) extinction values significantly higher than 1 are indicated.

The solar symbol ($\odot$) in the plot of Fig. 5 marks the position of the Galaxy. We have estimated it by applying the model of §3.1 and §3.2 to the Galactic integrated spectral emissivity, as shown in Figure 6. The Galaxy spectrum is well fitted by a pure cirrus emission with $\chi_c/\chi_\odot \simeq 7$. The estimated total dust mass turns out to be 10^7 $M_\odot$ while the optical depth $\tau \sim 0.3$. These values are somewhat lower than estimated by Sodroski et al. (1994), because of our different fit to the long-wavelength part of the spectrum (see comparison Fig. 6). The position of the Galaxy within the region occupied by the inactive galaxy population is consistent with our finding that the Galaxy's far-IR spectrum is dominated by cold *cirrus* emission.

Figure 7. The gas to dust mass ratio versus bolometric optical/mm luminosity (symbols as in Fig. 5). Mass of gas (including both HI and molecular gas) estimated from CO observations (see Andreani et al., 1995).

3.6 The dust-to-gas mass ratio

We report in Figure 7 a plot of the gas (HI + molecular, from Andreani et al., 1995) to dust ratio versus bolometric luminosity ($L_{bol} = L_O + L_{FIR}$). We first notice that the median $L_{bol} \sim 4.5\ 10^{10}\ L_\odot$ for the inactive objects is a factor 2.6 lower than the corresponding value for starbursts, consistent with our inference that the latter are characterized by an enhanced star-formation activity, hence higher luminosities. Second, the median gas/dust ratios for the two classes also differ on average ($< M_g/M_d > \simeq 400$ for the starbursts and $\simeq 1000$ for the inactive population). Finally, there is an apparent trend of $< M_g/M_d >$ to decrease with L_{bol} from values of 3000 to less than 400 for the inactive population.

The gas-to-dust ratio is particularly large ($\geq$3000) for three quite extended and close-by objects: 0300-23, 0045-25 (NGC 253) and 0128-22. The most likely explanation is that we have missed part of the dust emission, or underestimated the aperture correction to be applied (see §2.3), for 0300-23 and 0128-22, and it is probably even more so for the observations of NGC 253 by Chini et al. (1984) and by Krügel et al. (1990), whose photometry refers only to the inner region. In principle, it could be argued that these three objects are truly metal poor, but this is unlikely since CO emission were detected in all of them (Andreani, Casoli & Gerin 1995; Devereux & Young, 1990).

The position of the Galaxy in Figure 7 has been found by scaling the value of the ratio $< M_g/M_d >$ of Sodroski

et al. (1994) to be consistent with our lower estimated M_d. It is confirmed that the Galaxy tends to have a somewhat low gas-dust ratio, but the difference with respect to the median value of inactive galaxies of the same luminosity is now a factor 2, only marginally significant.

4 DISCUSSION

A fruitful combination of good sensitivity at long wavelengths, a large beam aperture and small angular size of the target objects, have allowed us to explore the dust content in galaxies down to the coldest possible temperatures and over a significant fraction of the optical galaxy extent.

Although our inferences on the millimetric size of galaxies have only a statistical sense, our results in Fig. 1 appear inconsistent with the assumptions that cold dust emission has a scale-length comparable to or larger than that of starlight. They rather suggest that the *mm* scale-length is somewhat smaller than the optical one, though is not possible to precisely quantify the difference until large bolometer arrays will be available.

From a detailed modelling of dust emission from a galaxy in which the dust is illuminated by an exponentially distributed radiation field, we conclude that our inferred difference between optical and *mm* lights corresponds to a dust distribution which is more centrally concentrated than the starlight, with a typical scale-length of one third of that of stars.

This effect may bear some relationship with the observed increase in metallicity towards the inner regions of galaxies (e.g. Issa et al. 1990; Sodroski et al., 1994; Carollo, Danziger, Buson, 1995) and with the idea of an enhanced past stellar activity there. A similar effect is seen in the Galaxy and in M31, where a dust-to-gas ratio increasing towards the inner Galactic regions is observed (Sodroski et al. 1995; Xu & Helou 1995). This fact is related by Sodroski et al. to the metallicity gradient as a function of the galactocentric distance (Panagia & Tosi, 1981; Shaver et al. 1983; Wilson & Rood 1994) observed in the Galaxy.

A published model (RR86, RR92) reproduces quite well the observed broad-band spectra (see Figures 2 and 4). According to their FIR/mm spectrum, a simple color criterion, supported by model predictions, allows us to classify these IR galaxies in two different groups: an *inactive* galaxy population, the we called *cirrus* dominated objects, and an active star-forming population, called *starbursts*.

The average galaxy FIR/mm spectrum can be fitted by a dust model including contributions from a cold and warm dust components, with the cold one bearing most of the dust mass. We find for the *median* galaxy in our sample a value of 1.9 10^7 $M_\odot$ in dust, only 2 percent of which is warm dust associated to star-forming regions.

We have tested the presence of very cold dust, still in the frame of the adopted dust model, by putting all dust components to the fundamental temperature of 3K (illuminating it with a very low radiation-field intensity). This, probably extreme, condition would increase the average dust mass to 3.5 10^7 $M_\odot$, 90% of which in very cold dust. We argue here that in the frame of the adopted dust model there is no large room for hidden cold dust and the estimation of the dust mass is quite robust.

It must be noted that estimation of the dust masses based on IRAS data *only* would produce values smaller by one order of magnitude. This was already noted by other authors. For instance, even indirect methods used to infer the amount of dust in galaxy disks, such as those based on the observed B-K and V-K colours, together with population synthesis models (Block et al. 1994), or the combination of FIR and UV data with a dust heating/cooling model (Xu and Helou, 1995), agree in finding dust amount larger than that inferred on the basis of the IRAS data alone. The dust mass evaluations for the two spirals NGC 4736 and NGC 4826 and for M31 are in agreement with the average dust mass found in the present work, while the gas-to-dust ratio is ~ 100, as in the Galaxy.

The average B-band optical depth along the line-of-sight, found by assuming that the total observed dust mass is confined within one third of the optical radius, spans a large range of values ($\tau_B = 0.1$ to 50, see Fig. 5). The largest values of dust mass, optical depth ($\tau_B > 1$) and of the dust/gas mass ratio are shared by objects characterized by a starbursting activity. The inactive "cirrus"-dominated galaxies, which are the typical population that bright optical samples select, seem to be not much obscured by dust.

These results are confirmed by an inspection of the *actual* A_B extinction values inferred from the observed ratio of optical to far-IR bolometric emissions. Relatively high values of A_B (> 1) are displayed only by a minority of the starbursting galaxies (6 out of 28 objects). Note, however, that for the latter class of sources the quantity A_B is probably quite a poor measure of the real extinction affecting the optical galaxy, since most of the far-IR emission there comes from starburst regions occupying very small volumes in the galactic body. In these cases too the average extinction is probably not larger than 1 mag.

There are some intriguing effects to notice in Fig. 7. The starbursting activity seems to imply a heavier dust enrichment of the ISM with respect to inactive spirals. The M_g/M_d median values are $\simeq 1000$ for the latter and 400 for the starbursts. The ongoing starburst may well have preprocessed the ISM in these objects significantly longer or more efficiently than inactive galaxies did.

The somewhat low M_g/M_d value found for the Galaxy in Figure 7 with respect to other *cirrus* dominated objects in our sample may be explained by the fact that the value of the ratio for the Galaxy mostly refers to the inner region, where most of the dust is concentrated, because such region is more strongly weighted in the observations of the Galactic emission. On the contrary, observations of external galaxies include the contribution of the outer dust-poor environments. So, we probably have to take into account a systematic bias when comparing gas-to-dust ratio measurements for the Milky Way and for distant galaxies.

Finally, there seems to be a trend favouring higher values of the mass in dust M_d relative to the total gas content M_g in higher luminosity *normal inactive* spirals. Assuming that this trend just reflects an increased metallicity, this effect parallels a similar trend of higher metallicities at higher masses inferred for galaxies of any morphological types (see a recent review in Edmunds and Terlevich 1992).

A number of abundance indicators, from the specific Mg_2 to the more general and widespread color-magnitude relationship, show that larger fractions of supernovae debris are re-

tained at greater galaxy masses (probably due to the deeper gravitational wall). An effect of this kind may be seen in our observations of the dust fraction in IR galaxies. The fact that starbursting galaxies in Fig. 7 do not follow the same relationship may be due to a much different history of metal production.

ACKNOWLEDGMENTS

Dave Clements is warmly thanked for taking the data of three objects. We are also grateful to Phil James, the referee of this paper, for his valuable comments and suggestions.

REFERENCES

Andreani P. 1994, ApJ 428, 447
Andreani P. & Franceschini A. 1992, A&A 260, 89
Andreani P., Casoli F. and Gerin M., 1995, A&A 300, 43
Block D., Witt A., Grosbol P., Stockton A., Moneti A. 1994, A&A 288, 383
Burstein D., Haynes M.P. & Faber S.M. 1991, Nat 353, 515
Chini R., Kreysa E., Mezger P.G., Gemünd H.P. 1984, A&A 137, 117
Chini R., Kreysa E., Krügel E., Mezger P.G., 1986, A&A 166, L8
Chini R. & Krügel E. 1993 A&A 279, 385
Chini R., Krügel E., Lemke R., Ward-Thompson D. 1995 A&A 295, 317
Choloniewski J. 1991, MNRAS 250 486
Conte N., 1993, Ph.D. Thesis, Padova University
Devereux N.A. & Young J.S. 1990, ApJ 359, 42
Disney, M., Davies, J., and Phillips, S., 1989: MNRAS 239, 939
Draine B.T., Anderson N. , 1985 ApJ 292, 494
Edmunds M. and Terlevich R. Eds., 1992 "Elements and the Cosmos", Cambridge University Press, Cambridge, UK
Franceschini A. & Andreani P. 1995, ApJ 440, L5
Giovannelli R., Haynes M.P., Salzer J.J., Wegner G., da Costa L.N., Freudling W., 1994 AJ 107, 2036
Huizinga J.E. & van Albada T.S. 1992 MNRAS 254, 677
James P.A. & Puxley P.J. 1993, Nat 363, 240
Kreysa E.: 1990, in *From Ground-Based to Space-Born Sub-mm Astronomy*, Proceedings of 29th Liège International Astrophysical Colloquium, **ESA SP-314**, p.265-270
Krügel E., Chini R., Klein U., Lemke R., Wielebinski R., Zykla R. 1990 A&A 240, 232
Lauberts A. & Valentijn E.A. *The Surface Photometry Catalogue of the ESO-Uppsala Galaxies*, European Southern Observatory, 1989
Mathis J.S., Mezger P.G., Panagia N. 1983, A&A 128, 212
Moshir M. et al., 1989, *Explanatory Supplement to the IRAS Faint Source Survey*, Pasadena:JPL
Peletier R.F., Valentijn E.A., Moorwood A.F.M., Freudling W., Knapen J.H., Beckman J.E. 1995, A&A in press
Rice W., Lonsdale C.J., Soifer B.T., Neugebauer G., Kopan E.L., Lloyd L.A. de Jong T., Habing H.J., 1988, ApJS 68, 91
Page, L., Cheng E., Meyer, S. 1990: ApJ 355, L1
Panagia N. & Tosi M., A&A 96, 306
Puget, J.L. 1989: report to the ISO Science Team.
Reid N, 1993, in *Galaxy Evolution: the Milky Way Perspective*, ASP Conference Series, Steven R. Majewski (ed.), 49, p.37
Rowan-Robinson, M., 1986: MNRAS 219, 737 (RR86)
Rowan-Robinson, M., 1992 MNRAS 258, 787 (RR92)
Shaver P. McGee R.X., Newton L.M., Danks A.C., Pottash S.R. 1983, MNRAS 204, 53
Smith B.J., Kleinmann S.G., Huchra J.P., Low F.J., 1987 ApJ 318, 161
Sodroski T.J., et al., 1994, ApJ 428 638
Sodroski T.J., et al., 1995, in COBE Workshop on *Unveiling the Cosmic Infrared Background*, College Park; COBE preprint No. 95-08
Stark A., Knapp G.R., Bally J., Wilson R.W. ,Penzias A.A., Rowe H.E. , 1986 ApJ, 310, 660
Thronson H., Walker C.K., Walker C.E., Maloney P., 1987, ApJ 318, 645
Xu, C., and De Zotti, G., 1989: A&A 225, 12
Xu, C., and Helou G., 1995, preprint
Valentijn E.A. 1994 MNRAS 266, 614
van Driel W., Valentijn E.A., Wesselius P.R., Kussendrager D. 1995 A&A 298, L41
Wainscoat R.J.,de Jong T., Wesselius P.R. 1987, A&A 181, 225
White R.E. & Keel W.C. 1992 , *Nat* 359, 129
Wilson T.L. & Rood R.T. 1994, ARA&A 32, 191
Wright E.L., et al. 1991, *ApJ* 381, 200

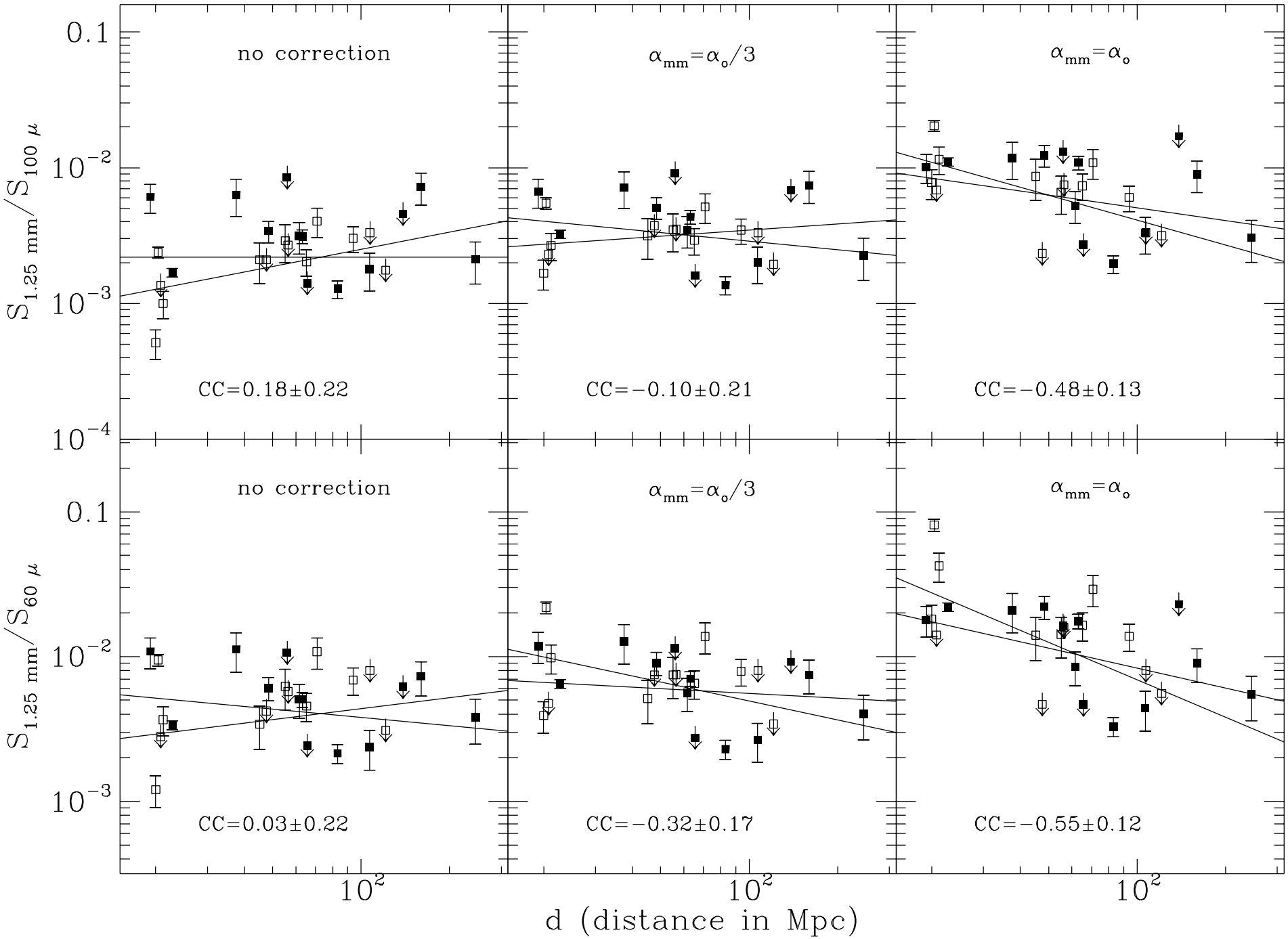
no correction
$\alpha_{mm}=\alpha_o/3$
$\alpha_{mm}=\alpha_o$
CC=0.18±0.22
CC=−0.10±0.21
CC=−0.48±0.13
no correction
$\alpha_{mm}=\alpha_o/3$
$\alpha_{mm}=\alpha_o$
CC=0.03±0.22
CC=−0.32±0.17
CC=−0.55±0.12
$S_{1.25\ mm}/S_{100\ \mu}$
$S_{1.25\ mm}/S_{60\ \mu}$
0.1
10^{-2}
10^{-3}
10^{-4}
10^2
d (distance in Mpc)

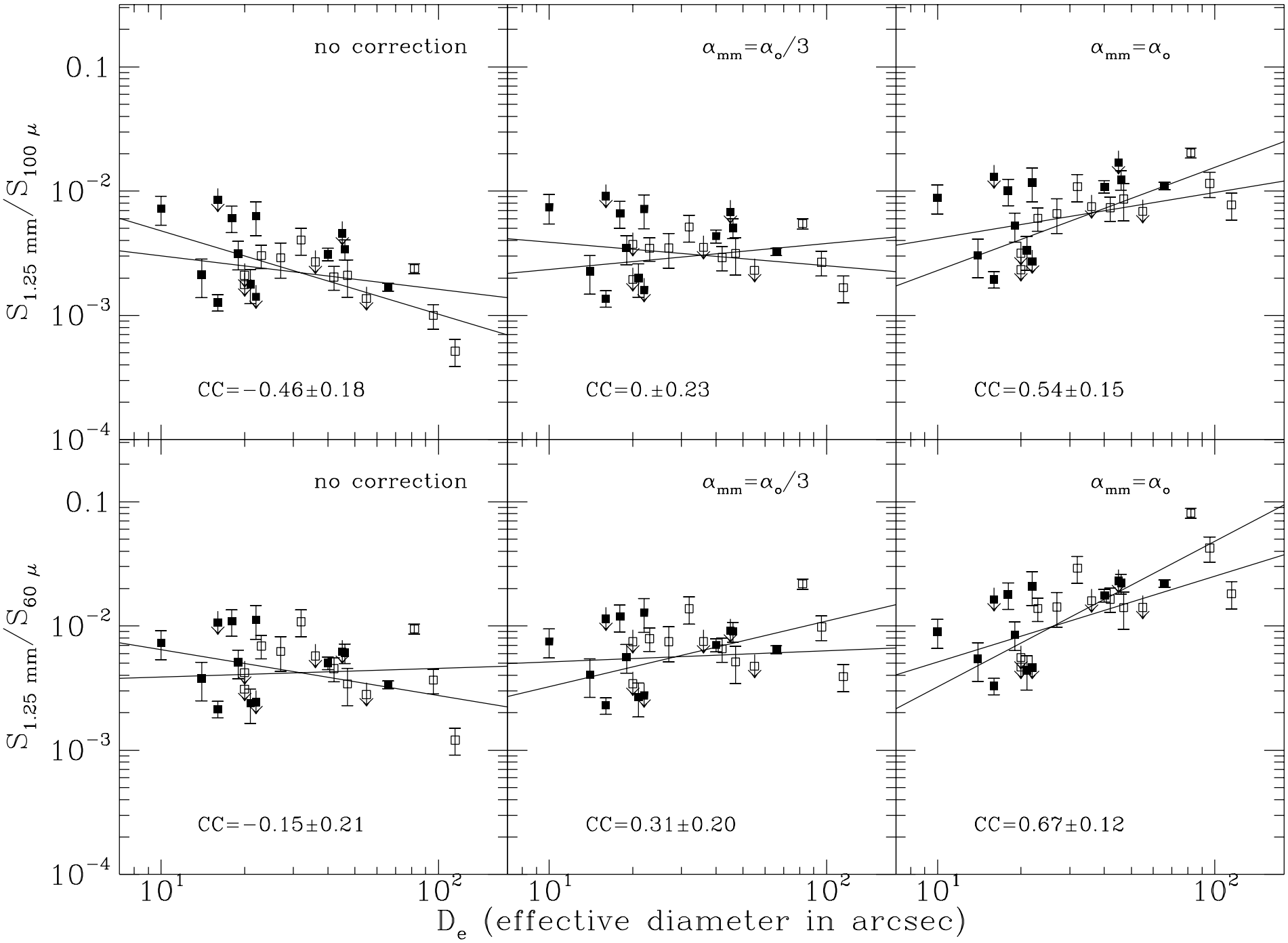
no correction
$\alpha_{mm}=\alpha_o/3$
$\alpha_{mm}=\alpha_o$
CC=−0.46±0.18
CC=0.±0.23
CC=0.54±0.15
CC=−0.15±0.21
CC=0.31±0.20
CC=0.67±0.12
$S_{1.25\ mm}/S_{100\ \mu}$
$S_{1.25\ mm}/S_{60\ \mu}$
0.1
10^{-2}
10^{-3}
10^{-4}
10^{1}
10^{2}
D_e (effective diameter in arcsec)

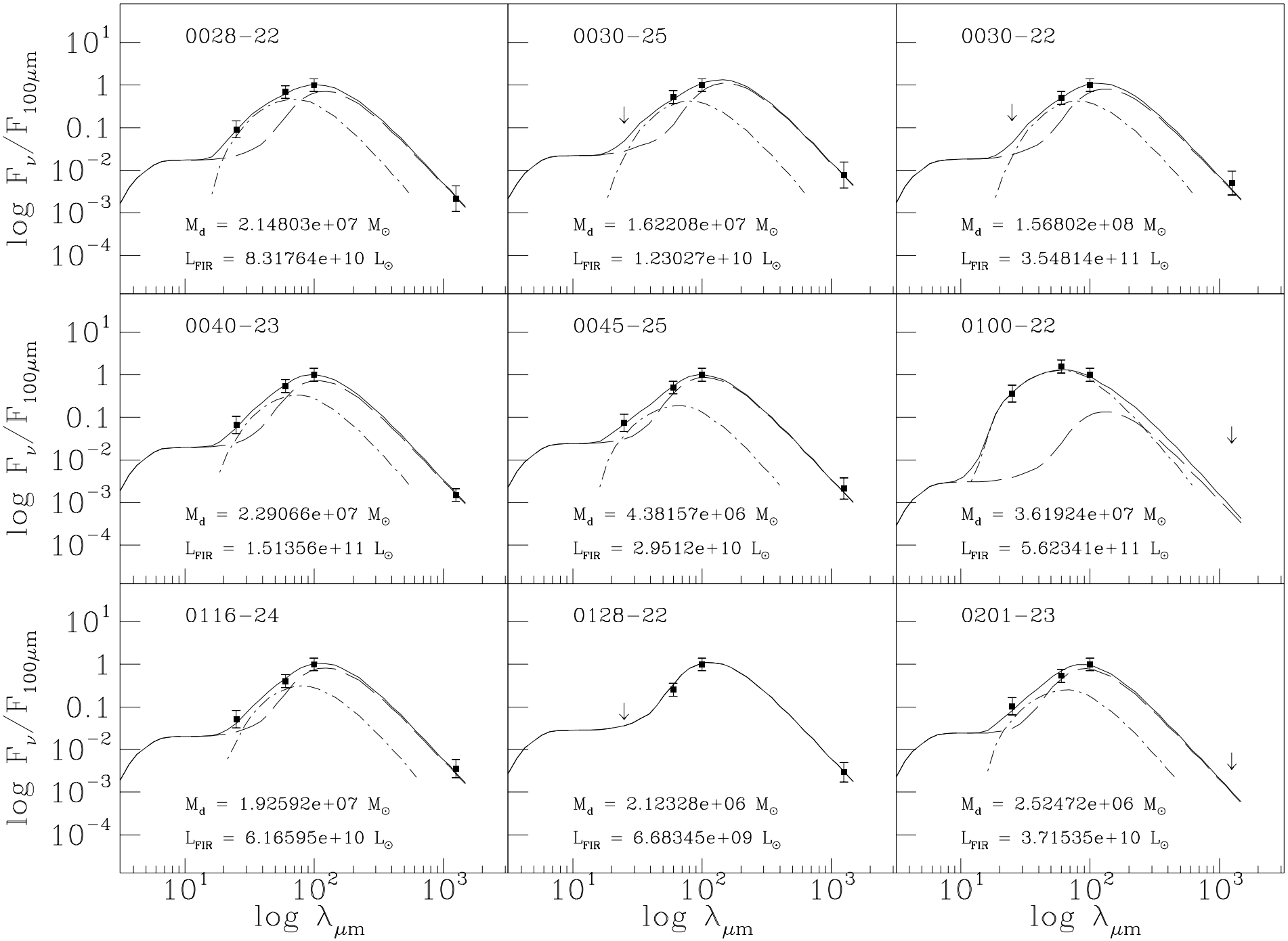
0028−22
M_d = 2.14803e+07 M_⊙
L_FIR = 8.31764e+10 L_⊙
0030−25
M_d = 1.62208e+07 M_⊙
L_FIR = 1.23027e+10 L_⊙
0030−22
M_d = 1.56802e+08 M_⊙
L_FIR = 3.54814e+11 L_⊙
0040−23
M_d = 2.29066e+07 M_⊙
L_FIR = 1.51356e+11 L_⊙
0045−25
M_d = 4.38157e+06 M_⊙
L_FIR = 2.9512e+10 L_⊙
0100−22
M_d = 3.61924e+07 M_⊙
L_FIR = 5.62341e+11 L_⊙
0116−24
M_d = 1.92592e+07 M_⊙
L_FIR = 6.16595e+10 L_⊙
0128−22
M_d = 2.12328e+06 M_⊙
L_FIR = 6.68345e+09 L_⊙
0201−23
M_d = 2.52472e+06 M_⊙
L_FIR = 3.71535e+10 L_⊙
log F_ν/F_100μm
log λ_μm

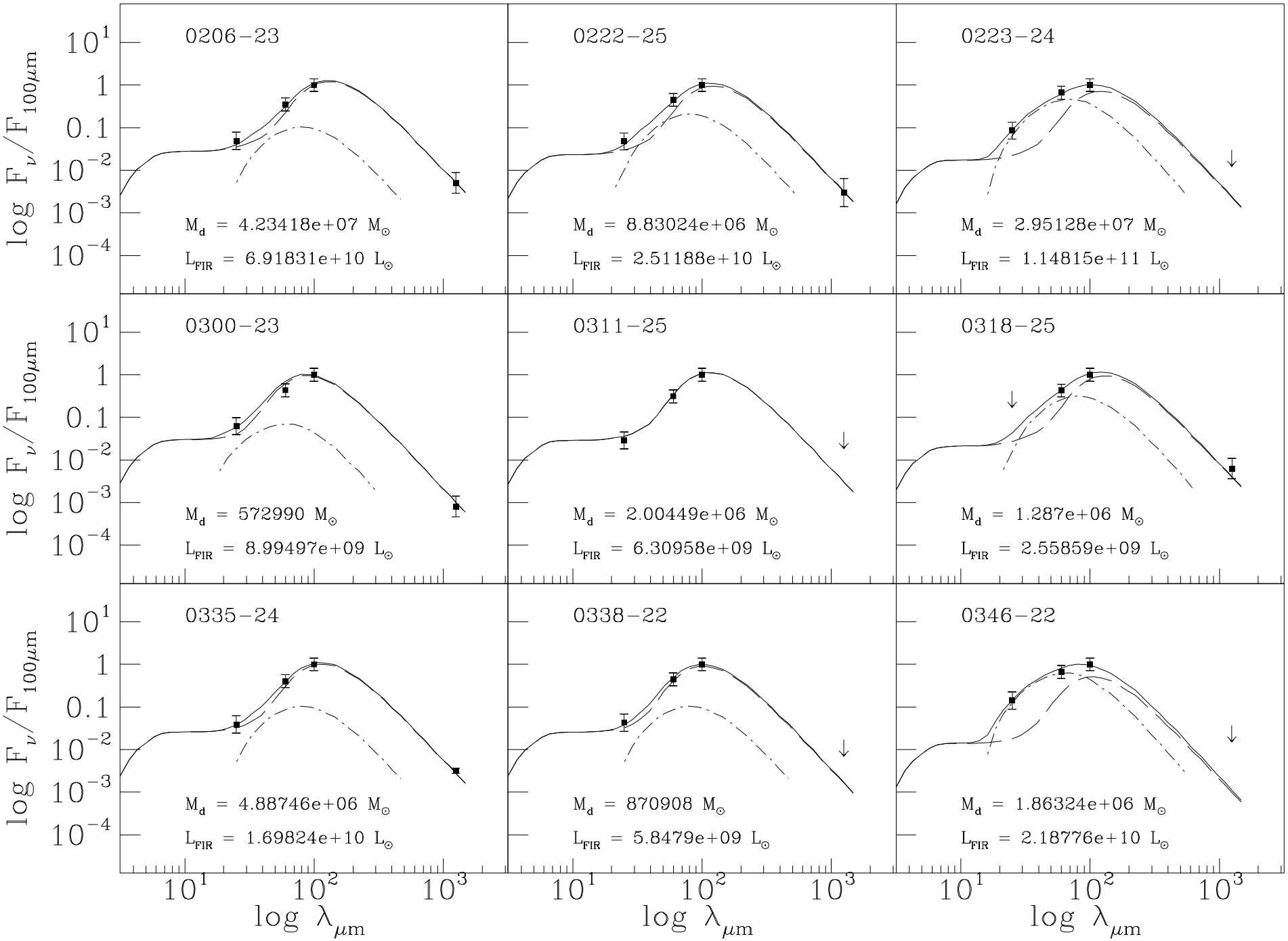
0206−23
M_d = 4.23418e+07 $M_\odot$
L_{FIR} = 6.91831e+10 $L_\odot$
0222−25
M_d = 8.83024e+06 $M_\odot$
L_{FIR} = 2.51188e+10 $L_\odot$
0223−24
M_d = 2.95128e+07 $M_\odot$
L_{FIR} = 1.14815e+11 $L_\odot$
0300−23
M_d = 572990 $M_\odot$
L_{FIR} = 8.99497e+09 $L_\odot$
0311−25
M_d = 2.00449e+06 $M_\odot$
L_{FIR} = 6.30958e+09 $L_\odot$
0318−25
M_d = 1.287e+06 $M_\odot$
L_{FIR} = 2.55859e+09 $L_\odot$
0335−24
M_d = 4.88746e+06 $M_\odot$
L_{FIR} = 1.69824e+10 $L_\odot$
0338−22
M_d = 870908 $M_\odot$
L_{FIR} = 5.8479e+09 $L_\odot$
0346−22
M_d = 1.86324e+06 $M_\odot$
L_{FIR} = 2.18776e+10 $L_\odot$
log $F_\nu/F_{100\mu m}$
log $\lambda_{\mu m}$

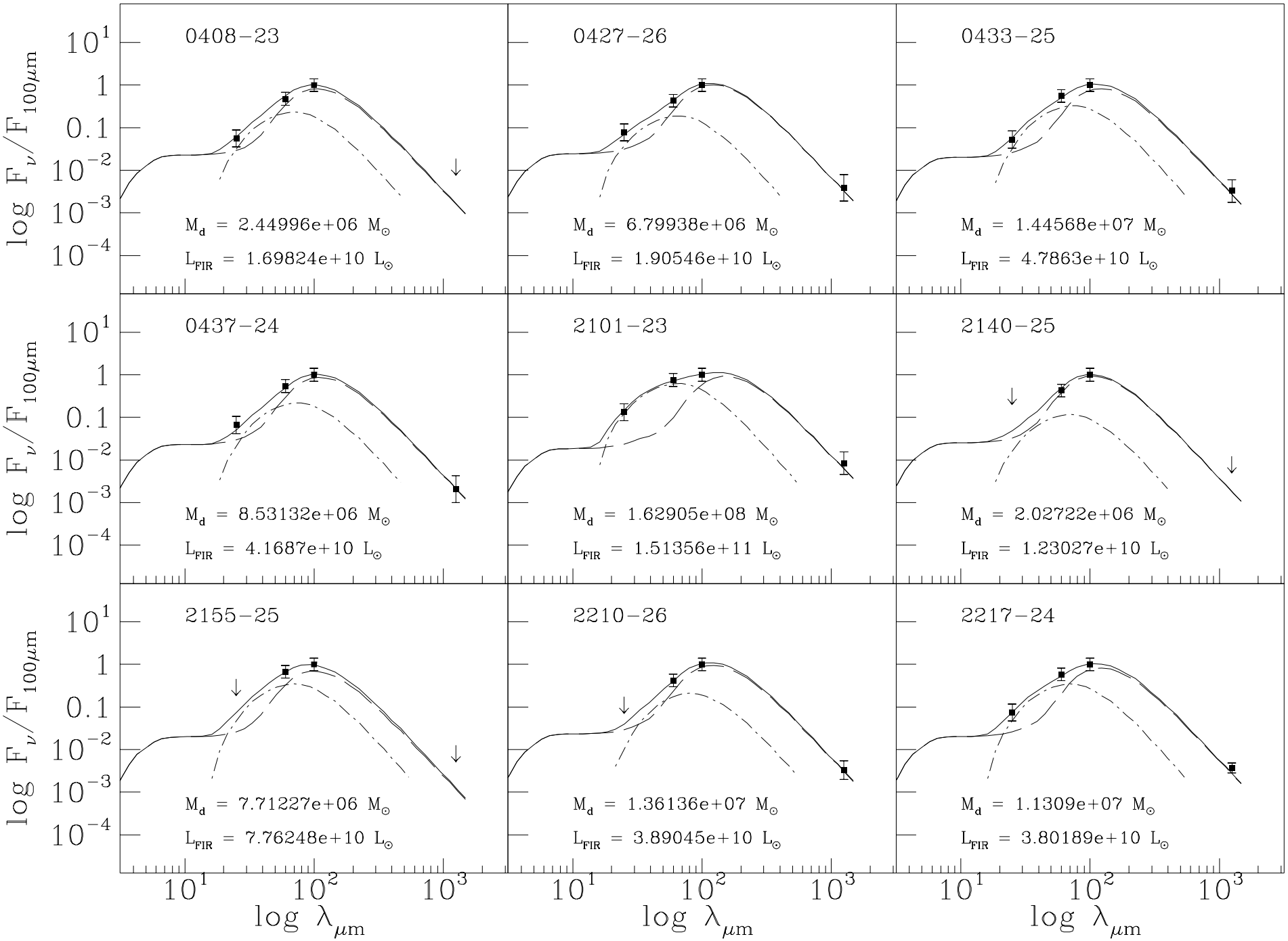
0408−23
M_d = 2.44996e+06 $M_\odot$
L_{FIR} = 1.69824e+10 $L_\odot$
0427−26
M_d = 6.79938e+06 $M_\odot$
L_{FIR} = 1.90546e+10 $L_\odot$
0433−25
M_d = 1.44568e+07 $M_\odot$
L_{FIR} = 4.7863e+10 $L_\odot$
0437−24
M_d = 8.53132e+06 $M_\odot$
L_{FIR} = 4.1687e+10 $L_\odot$
2101−23
M_d = 1.62905e+08 $M_\odot$
L_{FIR} = 1.51356e+11 $L_\odot$
2140−25
M_d = 2.02722e+06 $M_\odot$
L_{FIR} = 1.23027e+10 $L_\odot$
2155−25
M_d = 7.71227e+06 $M_\odot$
L_{FIR} = 7.76248e+10 $L_\odot$
2210−26
M_d = 1.36136e+07 $M_\odot$
L_{FIR} = 3.89045e+10 $L_\odot$
2217−24
M_d = 1.1309e+07 $M_\odot$
L_{FIR} = 3.80189e+10 $L_\odot$
log $F_\nu/F_{100\mu m}$
log $\lambda_{\mu m}$

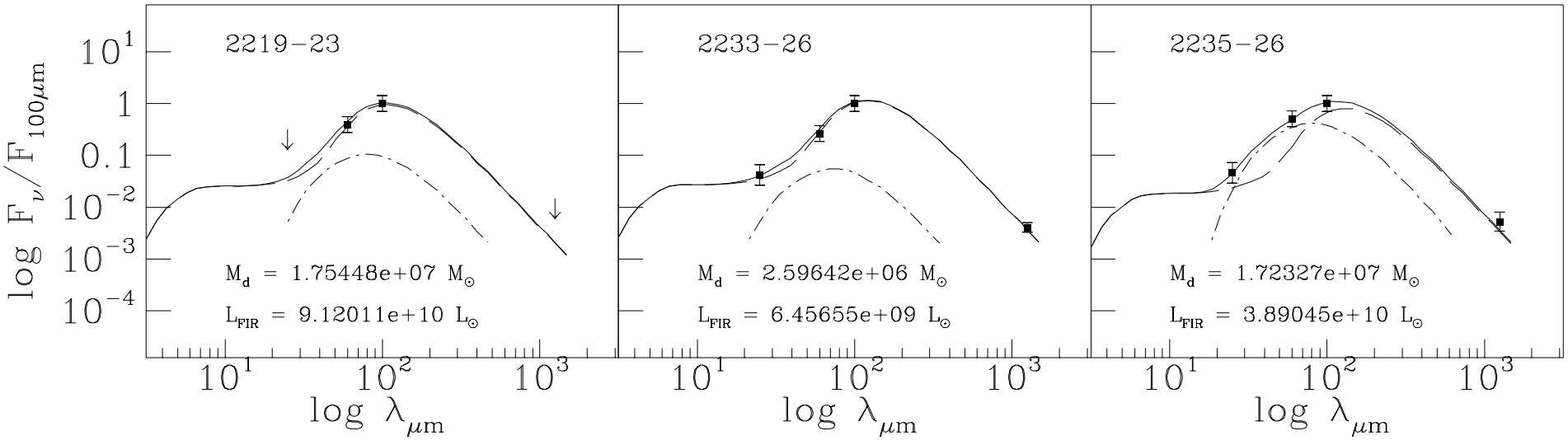
2219−23
2233−26
2235−26
M_d = 1.75448e+07 $M_\odot$
L_{FIR} = 9.12011e+10 $L_\odot$
M_d = 2.59642e+06 $M_\odot$
L_{FIR} = 6.45655e+09 $L_\odot$
M_d = 1.72327e+07 $M_\odot$
L_{FIR} = 3.89045e+10 $L_\odot$
log $F_\nu/F_{100\mu m}$
log $\lambda_{\mu m}$
10^1
1
0.1
10^{-2}
10^{-3}
10^{-4}
10^2
10^3

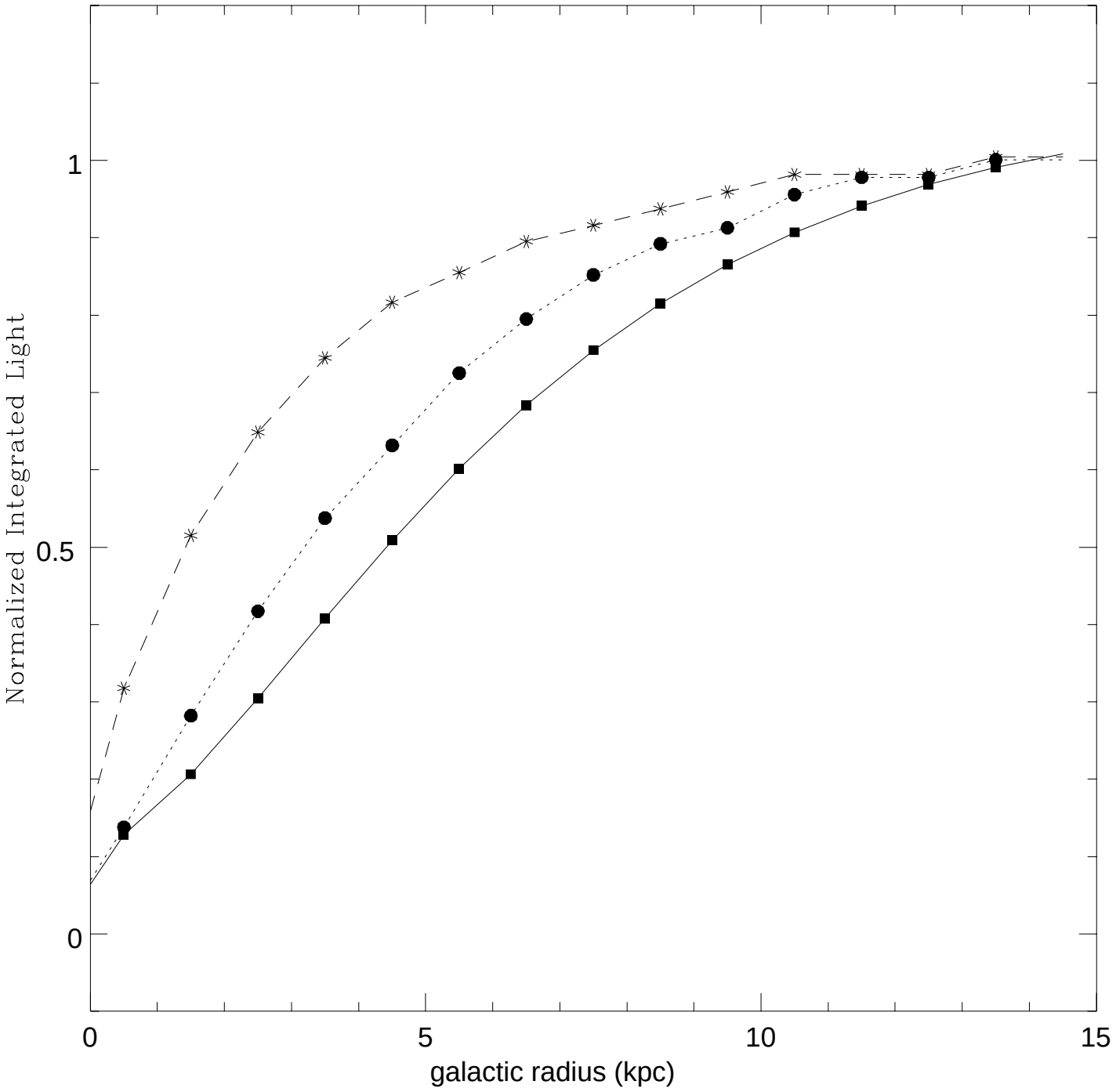
Normalized Integrated Light
1
0.5
0
0
5
10
15
galactic radius (kpc)

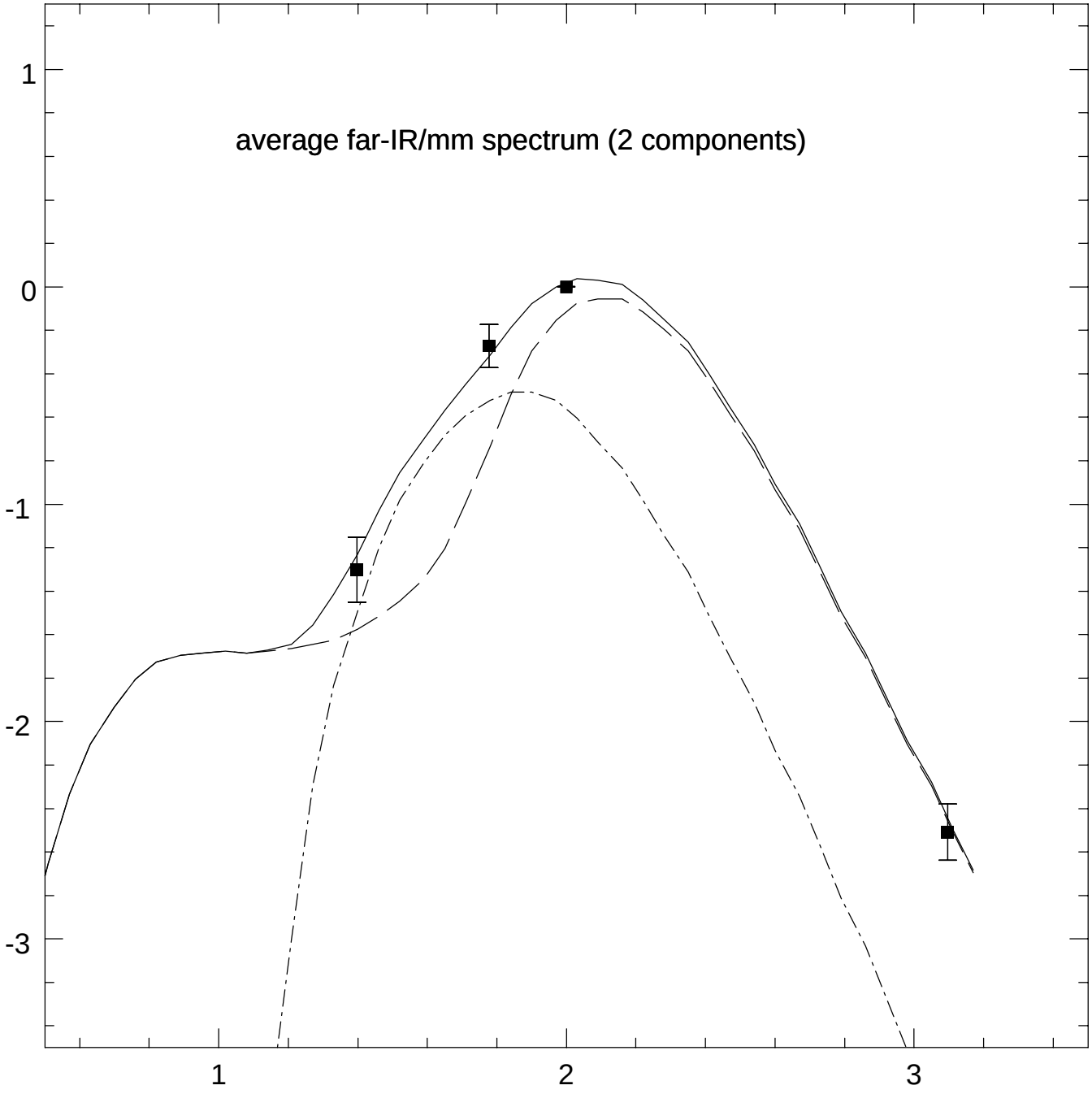
average far-IR/mm spectrum (2 components)
1
0
-1
-2
-3
1
2
3

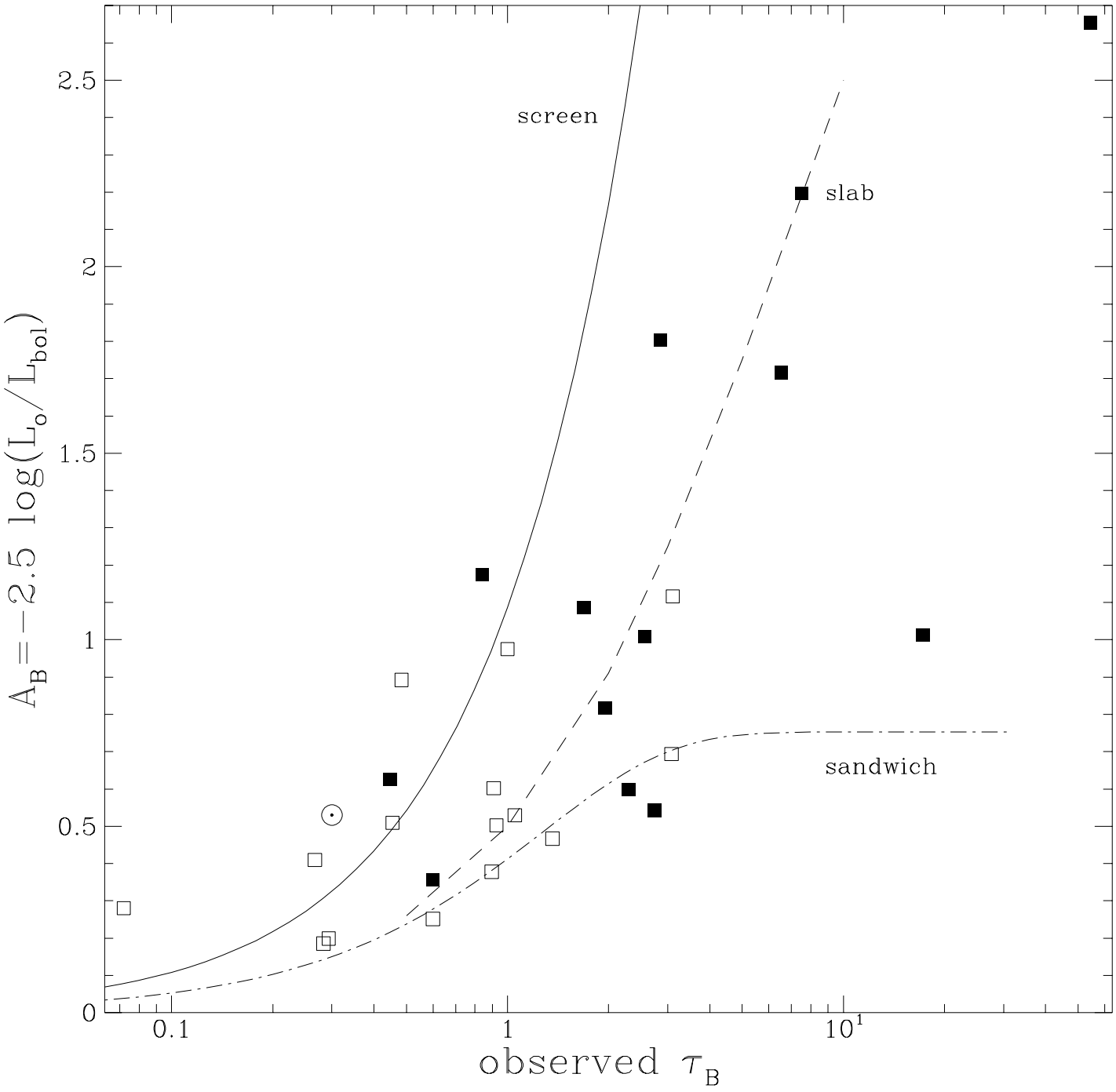
screen
slab
sandwich
$A_B = -2.5 \log(L_o/L_{bol})$
observed τ_B
0
0.5
1
1.5
2
2.5
0.1
1
10^1

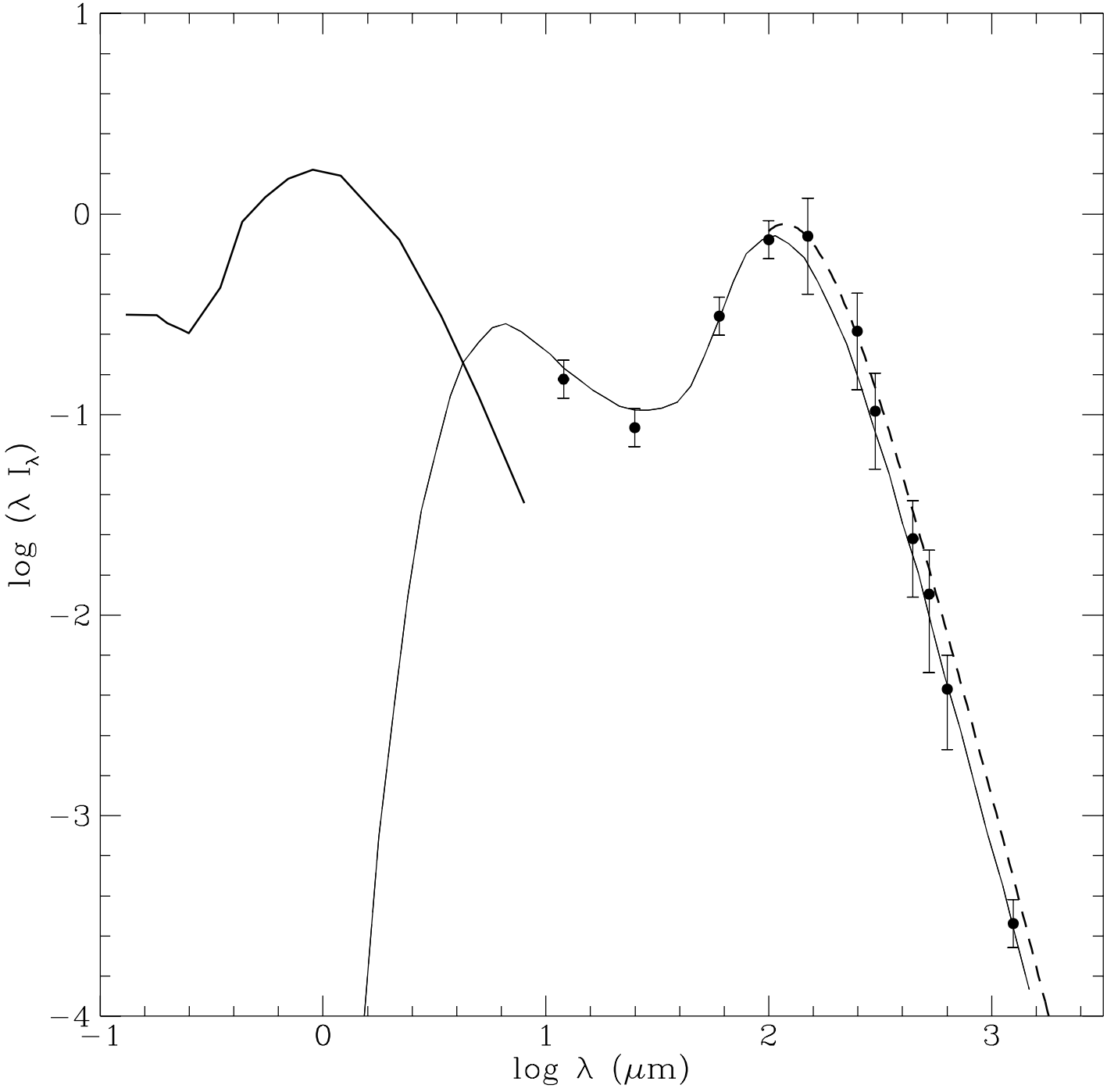
1
0
−1
−2
−3
−4
−1
0
1
2
3
log (λ I_λ)
log λ (μm)

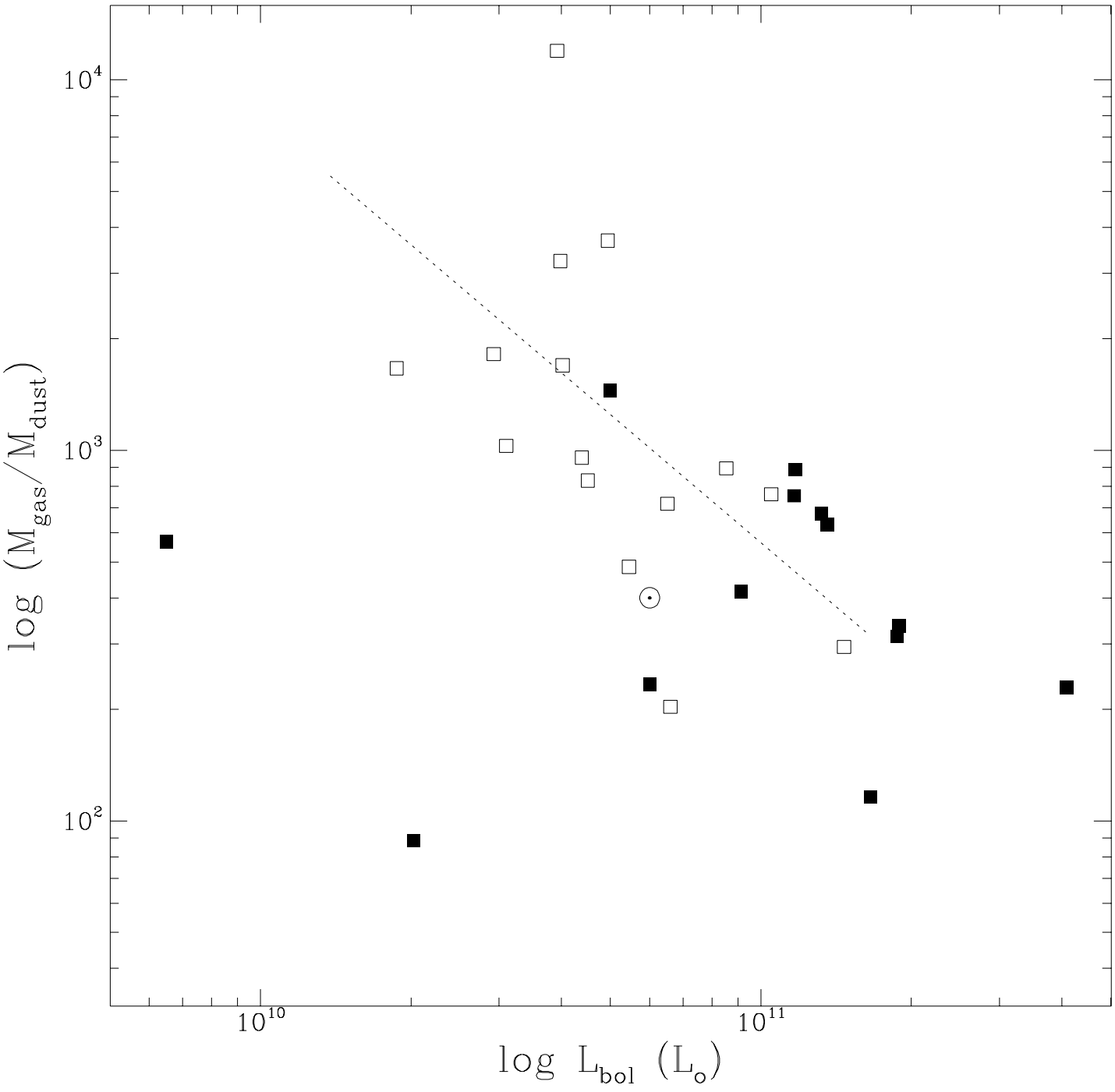
10^4
10^3
10^2
10^{10}
10^{11}
log (M_{gas}/M_{dust})
log L_{bol} (L_o)

Table 3. Physical parameters of the two-component dust model for the average galaxy spectrum [a]

Grain type	*cirrus* component (χ_c=11$\chi_\odot$)			*starburst* component (χ_c=120$\chi_\odot$)		
	T (K)	λ_{peak} (μm)	mass fraction (%)	T (K)	λ_{peak} (μm)	mass fraction (%)
30 μm amorph. carbon	6.8	616	8.6	11.3	400	0.2
0.1 μm amorph. silicates	22.1	144	45.8	37.0	79	1.2
0.1 μm amorph. carbon	23.5	144	14.6	37.0	79	0.4
0.03 μm silicates	26.1	123	11.7	57.7	60	0.3
0.01 μm silicates	26.7	123	1.9	70.4	45	0.1
0.03 μm graphite	30.6	123	6.3	57.7	60	0.2
0.01 μm graphite	31.0	123	3.4	70.4	45	0.1
2 $10^{-3}\mu m$ graphite	< 80	~ 50	2.6	–	–	–
5 $10^{-4}\mu m$ graphite	< 500	~ 10	2.6	–	–	–

Notes to Table 3

[a] The *average* galaxy has a spectral shape as in Fig. 43, a distance of 70 Mpc, and a flux $S_{100} = 5$ Jy. The total dust masses in the *cirrus* and *starburst* components are 2 $10^7 M_\odot$ and 3.4 $10^5 M_\odot$, respectively.

Table 1

optical properties of the sample

	IRAS position		Distance	optical photometry*			
name	R.A. (h)	δ °	D (Mpc)	A_e (")	D_{25} (")	m_B mag	morp. type
0028-22	00 28 38.0	-22 53 38	106.8	21.1	67.0	14.6	SB(s)b?pec
0030-25	00 30 10.8	-25 53 02	37.6	21.9	80.0	14.3	SA0
0030-22	00 30 48.9	-22 38 08	245.0	13.5	45.0	16.3	SBbc
0040-23	00 40 17.2	-23 49 57	83.2	15.7	52.0	14.4	SB(r)a
0045-25	00 45 5.2	-25 33 40	3.6	473.0	1799.0	8.2	SAB(s)c
0100-22	01 00 22.0	-22 38 09	471.2				Sy2
0116-24	01 16 22.0	-24 12 21	94.0	22.9	61.0	14.2	SB(r)ab
0128-22	01 28 03.7	-22 55 40	21.2	95.5	234.0	11.7	SAB(rs)c
0201-23	02 01 35.2	-23 33 14	65.6	21.6	75.0	14.1	(R)SB(r)bc
0206-23	02 06 59.9	-23 39 04	70.8	32.4	110.0	13.2	Sbc
0222-25	02 22 49.5	-25 00 53	45.2	47.3	132.0	12.5	SB(s)cd
0223-24	02 23 42.4	-24 56 03	138.8	20.4	65.0	15.2	(R)SB(r)a
0300-23	03 00 23.7	-23 03 43	18.5	115.0	313.0	11.3	SB(r)c
0311-25	03 11 22.0	-25 54 29	22.4	94.4	237.0	11.8	S...
0318-25	03 18 53.5	-25 41 29	19.2	18.2	65.0	13.6	Sb
0335-24	03 35 19.7	-24 39 48	19.9	66.1	219.0	11.6	SB(s)cd
0338-22	03 38 45.6	-22 43 29	20.8	55.0	188.0	12.5	(R)SAB(s)
0346-22	03 46 47.5	-22 16 59	56.0	15.5	72.0	13.8	(R)SBa
0408-23	04 08 14.7	-23 44 46	56.4	35.9	129.0	13.8	S0/a
0427-26	04 27 28.4	-26 49 12	55.2	26.9	77.0	13.5	SB(r)ab
0433-25	04 33 35.0	-25 14 05	61.6	18.6	81.0	14.9	Sb
0437-24	04 37 00.9	-24 16 52	56.0	21.4	67.0	14.0	Sb
2101-23	21 01 16.5	-23 38 03	160.0	10.0	16.8	16.8	merger?
2140-25	21 40 44.2	-25 35 06	47.6	20.0	100.0	14.0	Sb
2155-25	21 55 26.5	-25 07 32	121.1	20.0	51.0	15.1	(R)SBa
2210-26	22 10 18.8	-26 23 49	65.2	42.0	123.0	13.2	SA(s)0/a
2217-24	22 17 57.9	-24 55 50	63.2	40.0	117.0	12.7	(R)SA(r)0
2219-23	22 19 35.1	-23 20 13	107.2				S r
2233-26	22 33 00.8	-26 18 31	18.9	82.0	274.0	11.5	SAB(rs)bc
2235-26	22 35 56.3	-26 06 38	48.4	46.0	173.0	12.8	SA(s)ab

* *optical photometry taken from ESO-LV data base*

Table 2

IRAS and mm fluxes of the sample

name	IRAS fluxes (mJy)			$1.25mm$ fluxes (mJy)					
	(1) $S_{25\mu m}$	(2) $S_{60\mu m}$	(3) $S_{100\mu m}$	(4) $S_{1.25mm}$	(5) σ_{mm}	(6) $S^{c}_{1.25mm}$	(7) σ^{c}_{mm}	(8) $S^{c'}_{1.25mm}$	(9) $\sigma^{c'}_{mm}$
0028-22	494.5	3690.3	5375.5	10.3	3.1	11.6	3.5	19.1	5.7
0030-25	<305.8	2404.8	4609.8	31.0	9.4	35.7	10.8	57.8	17.5
0030-22	<315.8	2063.4	4151.4	19.6	5.5	20.8	5.8	28.1	7.9
0040-23	1188.5	9804.2	18032.8	25.4	3.8	27.2	4.1	38.8	5.8
0045-25	13789.0	93169.0	186167.0	4400.0⋆	1700.0				
0100-22	517.9	2263.8	1448.0	<18.8					
0116-24	271.2	2128.2	5264.8	16.3	3.5	18.7	4.0	32.6	7.0
0128-22	<318.8	3062.5	12062.3	13.1	3.0	35.2	8.1	151.2	34.6
0201-23	760.6	3932.7	7279.8	<11.4		<13.0		<21.9	
0206-23	455.4	3251.9	9252.3	36.8	8.9	46.9	11.3	99.2	24.0
0222-25	443.4	4158.2	9289.9	18.3	6.1	27.7	9.2	75.6	25.2
0223-24	371.5	2886.7	4367.2	<18.9		<28.0		<70.3	
0300-23	1432.4	9852.0	22849.6	12.1	3.0	18.5	4.5	48.6	12.1
0311-25	290.5	3165.7	10187.4	36.9	0.0	98.5	0.0	417.3	0.0
0318-25	<428.1	2047.1	4824.9	27.8	6.7	30.4	7.3	45.9	11.1
0335-24	1341.0	14034.8	34428.6	91.0	5.5	108.5	6.6	203.9	12.3
0338-22	506.5	5258.1	11773.5	<25.2		<42.5		<126.9	
0346-22	736.4	3429.7	5186.8	<37.6		<40.4		<57.8	
0408-23	246.5	2101.6	4434.6	<13.3		<17.6		<39.0	
0427-26	356.0	1977.0	4602.0	14.8	4.6	17.7	5.5	33.7	10.5
0433-25	492.3	5216.4	9356.1	27.7	7.3	30.6	8.1	46.5	12.3
0437-24	716.7	5889.5	10875.3	19.6	6.2	22.2	7.0	36.4	11.5
2101-23	405.0	2325.5	3086.3	25.3	6.7	26.0	6.9	31.2	8.3
2140-25	<483.0	1966.3	4656.2	<10.7		<12.0		<19.2	
2155-25	<419.9	2964.8	4390.5	<10.6		<11.8		<18.7	
2210-26	<254.1	2879.1	6885.7	15.9	3.5	22.8	5.0	57.5	12.7
2217-24	517.1	4060.2	6997.3	24.0	2.8	25.8	3.0	37.1	4.3
2219-23	<448.5	2613.0	6676.1	<20.8					
2233-26	600.7	3774.8	14353.2	44.8	4.1	57.8	5.3	122.3	11.2
2235-26	540.1	5917.3	11708.6	40.0	7.3	61.1	11.2	145.5	26.6

col. (4) and (5) no beam aperture correction
col. (6) and (7) beam aperture correction with $\alpha_{mm} = \alpha_o/3$
col. (8) and (9) beam aperture correction with $\alpha_{mm} = \alpha_o$
⋆ mm photometry taken from Chini et al. 1984